Force-induced repolarization of an active crawler

Pierre Recho, Thibaut Putelat, Lev Truskinovsky

Force-induced repolarization of an active crawler

Pierre Recho[1]

[1]LIPhy, CNRS–UMR 5588, Université Grenoble Alpes, F-38000 Grenoble, France

E-mail: pierre.recho@univ-grenoble-alpes.fr

Thibaut Putelat[2,3]

[2]DEM, Queen's School of Engineering, University of Bristol, Bristol, BS8 1TR, United Kingdom
[3] SAS, Rothamsted Research, Harpenden, AL5 2JQ, United Kingdom

E-mail: thibaut.putelat@rothamsted.ac.uk

Lev Truskinovsky[4]

[4]PMMH, CNRS–UMR 7636, ESPCI ParisTech, F-75005 Paris, France

E-mail: lev.truskinovsky@espci.fr

Keywords: cell crawling, active gel, active particle, force velocity relation, contact inhibition of locomotion. Submitted to: *New J. Phys.*

Abstract. We develop a quantitative model of mechanical repolarization in a contraction-driven gel layer mimicking a crawling cell. We show that the force-velocity relations for such active crawlers exhibit multi-valuedness and hysteresis under both force and velocity control. The model predicts steady oscillations of cells attached to an elastic environment and offers a self-consistent mechanical explanation for all experimentally observed outcomes of cell collision tests.

Introduction

To perform individual tasks, for instance, chase an intruder, or to act collectively, as in morphogenetic flows, crawling cells are able to switch their direction of motion in response to external stimuli. They do so by reorganizing their cytoskeleton [1], an internal meshwork of biopolymers held together by passive crosslinkers and actively contracted by molecular motors. Among the various physical cues that can induce the implied repolarization [2, 3], mechanical contact forces are particularily important when cells operate in crowded environments.

Building reliable links between repolarization mechanisms and measurable biophysical parameters is fundamental for the control of development, integrity and

regeneration of living organisms [4–13]. A broadly accepted mechanism of force-induced repolarization relies on reaction-diffusion instability involving several biochemical agents, in particular, Rho-GTPase, which controls the motor activity in the cytoskeleton [14–16]. In this paper we propose an alternative mechanism by showing that the application of an external force can lead directly to mechanical repolarization involving relocation of molecular motors, without invoking any biochemical signal transduction.

We build our theoretical construction upon the recent advances in the modeling of individual cell migration [17–22]. As a proof of principle, we use an analytically transparent one-dimensional model of an active gel representing the cytoskeleton as a contraction driven viscous layer [23–26]. Such prototypical model is appropriate for the case of a cell crawling on a 1D track [27] or inside a capillary [28]. Interestingly, it has been recently argued that motility confined to such 1D objects may be closer to the physiological 3D motility along fibers of the extra-cellular matrix than 2D motility on a flat substrate [29, 30].

To make quantitative predictions, we consider two basic problems: the oscillatory behavior of an elastically tethered cell and the head-on collision of two initially polarized self propelling cells. Our results highlight two important qualitative features of the proposed model. First of all, at a fixed value of the external force the model supports two coexisting steady regimes: *dissipative*, when the active object is dragged by the force, and *anti-dissipative*, when it is pulling cargo. The fact that the cytoskeleton can spontaneously self-organize from one of these steady states to another through a hysteresis loop offers a purely mechanical explanation for cell repolarization. However, this would not be enough, for instance, in dealing with cell collision. Here we use another important feature of the model, that a steady regime with a given velocity can take place under applied forces of *opposite* signs, corresponding to either an attached cargo or an external engine. In particular, our active segment can be stalled by two forces that are equal in magnitude but have different directions.

The importance of the study of spontaneous activity-induced mechanical oscillations stems from their ubiquitous presence in living systems at various length-scales [31, 32]. Contractility due to the presence of molecular motors has been identified as one of the main mechanisms behind this phenomenon [33, 34]. In particular, contractility-driven center of mass oscillations have been recently reported for cells constrained to move along one-dimensional fibers [35]. Here we show that our simple model predicts such steady state oscillations in the case of tethered cells when both the contractility and the stiffness of the effective spring are within a physiological range. We construct a phase diagram in the space of measurable parameters which distinguishes the oscillatory regimes from the regimes when the cell is either static, unable to polarize, or fully polarized but stalled by the contact force.

Another important test of any theory of cell motility is its ability to capture adequately the repolarization caused by the mechanical interaction between colliding cells. Experiments show that collision of two cells can result in four basic outcomes [36, 37]: velocity reversal, representing a quasi-elastic collision with symmetric

repolarization, two quasi-inelastic pairing scenarios with the formation of a cell doublet that can be motile (train) or static (stall) and finally, a bypass regime, when cells advance over each other [16]. The reversal and pairing regimes can be linked to with the phenomenon of *contact inhibition of locomotion* (CIL) [38]. Being a driver of cell dispersion and collective motility, CIL is crucial within biological tissues and its loss is usually associated with pathological processes, including cancer [38]. Motivated by experimental observations which suggest that a fundamental building block of CIL is motor-induced contractility [39], we simulated cell collision tests using our active layer model. It is quite remarkable that all four known cell collision scenarios could be accessed in this purely mechanical setting by tuning a single nondimensional parameter describing cell contractility. The obtained phase diagram reveals the physical conditions ensuring the failure of CIL, which have so far remained largely unknown.

To emphasize the importance of the force-induced repolarization in problems involving multiple cell collisions, we developed a reduced model of our active *segments* viewing them as active *particles* with polarity serving as an internal parameter. Despite the extreme simplicity of such a scaled-down model, which reduces to a system of two ODE (instead of the original system of PDE), we show that it captures all the steady and non-steady regimes which we have identified in the original active layer model.

Model of a crawling segment

We represent a cell crawling on a straight track by a segment of viscous contractile gel of length L, see the inset in Fig. 1.

To make the problem analytically tractable, we assume that the length of such active segment L is fixed. The associated size-control mechanisms are discussed in [40]. While length changes are known to be involved in oscillatory motion of cells [41] and may play some role during the initiation of motility [42], we have chosen to neglect these effects in the present paper in order to study the mechanical repolarization phenomenon in its most pure form. We also note that in the special case of fish keratocytes, the cell length is tightly controlled during the motion and the stiffness of an effective "spring", ensuring such a control, is much larger than the stresses involved in the rearrangements of the cytoskeleton [40, 43].

The time dependent free boundaries of the cell are then $x_f(t)$ for the front and $x_r(t) = x_f(t) - L$ for the rear. Using the position of the geometric center of the segment $S(t) = (x_r(t) + x_f(t))/2$ as a reference, we can introduce the co-moving coordinate $y(x,t) = x - S(t) \in [-L/2, L/2]$. Given that the segment boundaries are impermeable, we can write

$$V(t) = \partial_t S = \partial_t x_{r,f} = w(\pm L/2, t), \tag{1}$$

where V is the macroscopic velocity of the segment and $w(y,t)$ is the microscopic velocity of the cytoskeleton in the co-moving frame of reference.

Linear momentum balance for the cytoskeleton requires that

$$\partial_y \sigma = \xi w, \tag{2}$$

where $\sigma(y,t)$ is the axial stress field and ξ is the external friction coefficient. The constitutive model of the active gel reduces in this 1D setting to a relation

$$\sigma = \eta \partial_y w + \chi c, \tag{3}$$

where η is the bulk viscosity, χ is the contractility and $c(y,t)$ is the concentration of motors generating the active stress.

Following [44], we assume that the symmetry is broken by the applied force $F(t)$ which enters the model through the boundary condition

$$\sigma(L/2,t) - \sigma(-L/2,t) = F. \tag{4}$$

Note that condition (4) does not depend on the exact configuration/partition of the external loading at the two boundaries of the segment. Indeed, if we denote $q_\pm$ the applied tractions at the $\pm L/2$ and introduce q_0 the (kinematic) residual stress associated with the length constraint, we obtain two conditions $\sigma(\pm L/2,t) = q_\pm + q_0$ at the expense of introducing an additional unknown function. If we eliminate q_0 we obtain (4) with $F = q_+ - q_-$.

Following [26, 45], we further assume that the organization of the molecular motors in the segment is governed by the drift-diffusion equation

$$\partial_t c + \partial_y[c(w - V)] = D\partial_{yy} c,$$

which is equipped with no flux boundary conditions $\partial_y c(\pm L/2,t) = 0$, ensuring that the total amount of motors $M = \int_{-L/2}^{L/2} c dy$ remains a constant.

To non-dimensionalize the problem we introduce the characteristic length $\bar{l} = \sqrt{\eta/\xi}$, time $\bar{t} = \bar{l}^{\,2}/D$, concentration $\bar{c} = M/L$, stress $\bar{\sigma} = \xi D$ and velocity $\bar{v} = \bar{l}/\bar{t}$. The ensuing problem depends on three dimensionless parameters, $\mathcal{L} := L/\bar{l}$, $F := F/\bar{\sigma}$ and $\mathcal{P} = M\chi/(\bar{l}\bar{\sigma})$, representing, respectively, the normalized, length of the segment, traction force applied to the system and contractility of the motors. In the context of fish keratocytes, available data lead to the following basic estimates [40]: $\mathcal{P} \sim 10$ and $\mathcal{L} \sim 2$ but these numbers can vary depending on experimental conditions [45].

In the obtained model the flow velocity w at point y is induced by the presence in another point z of an active force dipole, represented by a motor concentration-dependent active stress [23, 24, 46]. It is also affected by the external force F. If we combine the momentum balance with the constitutive relation we can combine these two effects in a single relation

$$w(y,t) = \mathcal{P}\phi * c(y,t) + F(t)\partial_y \phi(y - \mathcal{L}/2). \tag{5}$$

Here we introduced the convolution operator

$$\phi * c(y,t) = \mathcal{L}^{-1} \int_{-\mathcal{L}/2}^{\mathcal{L}/2} \phi(y-z) c(z,t) dz.$$

The kernel

$$\phi(y) = \sinh\left(y + \mathcal{L}/2\right) / \left[2\sinh(\mathcal{L}/2)\right] - H(y)\cosh\left(y\right),$$

where $H(y)$ is the Heaviside function, is an odd function which ensures that an even distribution of force dipoles does not generate a directional flow [47].

Velocity-Force relation

Under the action of a constant external force F, the active layer reaches a steady velocity V which can be found by solving the stationary drift-diffusion equation ($\partial_t c = 0$) with the nonlocal closure relation (5). The ensuing velocity-force (V-F) relations are illustrated in Fig. 1. The $\mathcal{L}$ dependence of the critical thresholds is shown in Fig. 2.

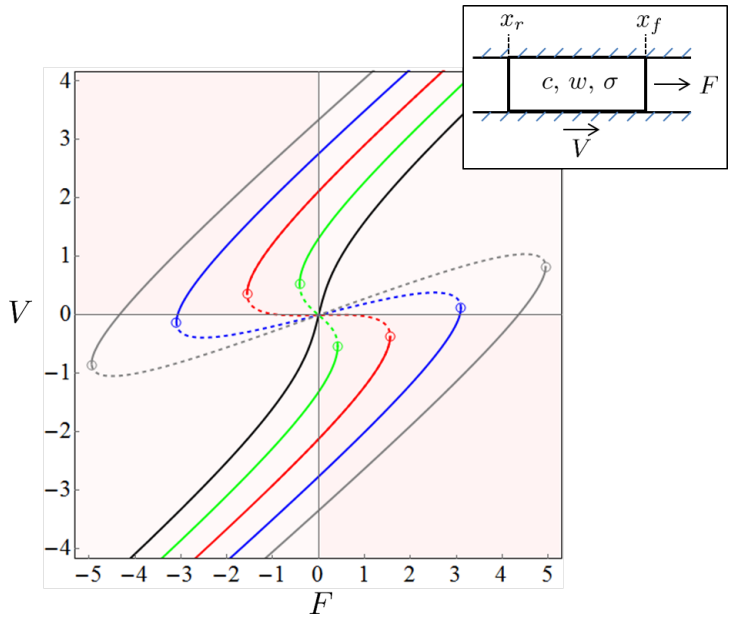

Figure 1. Four basic types of V-F relations for a crawling active segment. The dashed parts of the V-F curves correspond to unstable regimes. Parameter $\mathcal{L} = 2$ is fixed, producing the critical thresholds $\mathcal{P}_c \simeq 5.3$, $\mathcal{P}_m \simeq 6.9$ and $\mathcal{P}_s \simeq 7.8$. The V-F curves are plotted for $\mathcal{P} = 5 \leq \mathcal{P}_c$ (black), $\mathcal{P}_c \leq \mathcal{P} = 6 \leq \mathcal{P}_m$ (green), $\mathcal{P}_m \leq \mathcal{P} = 7 \leq \mathcal{P}_s$ (red) and $\mathcal{P}_s \leq \mathcal{P} = 8, 9$ (blue, gray). The darker background indicates the region where the V-F curve is anti-dissipative.

When $\mathcal{P}$ is smaller than $\mathcal{P}_c(\mathcal{L})$, the V-F relations are single-valued and dissipative, in the sense that $VF > 0$. In these regimes, when the velocity V is large and $\mathcal{P} \ll F$, the effective drag coefficient (tangential viscosity) is always positive and $\mathcal{P}$ independent

$$\mu_\infty = \partial_V F|_{V=\infty} = 2\tanh(\mathcal{L}/2) > 0.$$

When V is small, such drag coefficient depends on $\mathcal{P}$, in particular,

$$\mu_0 = \partial_V F|_{V=0} = (\mathcal{L}/\omega)^3 \left(2\tanh\left(\omega/2\right) - (\mathcal{P}/\mathcal{L})\omega\right),$$

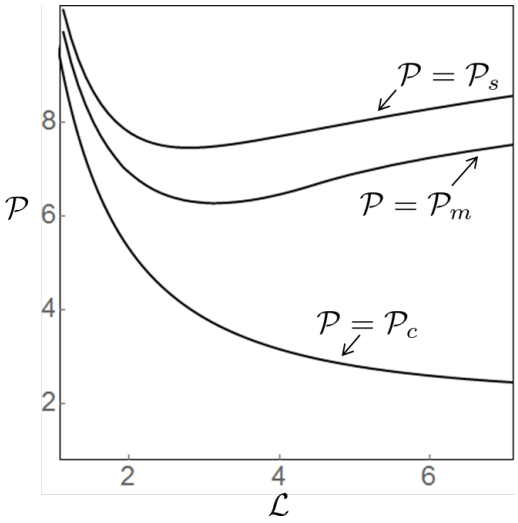

Figure 2. Dependence of the three thresholds $\mathcal{P}_c$, $\mathcal{P}_m$ and $\mathcal{P}_s$ on the parameter $\mathcal{L}$.

where $\omega^2 = \mathcal{L}^2\,(1 - \mathcal{P}/\mathcal{L})$. Overall, the increase of contractility reduces the effective drag until μ_0 vanishes at $\mathcal{P} = \mathcal{P}_c$. Similar effect of activity on friction has been reported for several other systems as well [48, 49].

When $\mathcal{P} > \mathcal{P}_c$, the V-F relation develops a domain of bi-stability which spreads over the range $F \in [-F_t, F_t]$. Within this range, the stationary velocity can take three values, $V_0^* < V_0 < V_0^{**}$; the metastable branches $V_0^*(F)$ and $V_0^{**}(F)$ are connected through an unstable branch $V_0(F)$.

Note that between the two turning points $F = \pm F_t$ one of the metastable dynamic regimes is necessarily anti-dissipative in the sense that $VF \leq 0$. In such regimes molecular motors overcome the passive frictional and viscous dissipation.

To clarify this point, consider the energy balance relation :

$$\frac{FV}{\mathcal{L}} = \int_{-\mathcal{L}/2}^{\mathcal{L}/2} [w^2 + (\partial_y w)^2] dy + \frac{\mathcal{P}}{\mathcal{L}} \int_{-\mathcal{L}/2}^{\mathcal{L}/2} c \partial_y w dy. \tag{6}$$

which can be obtained by multiplying (2) by (3) and integrating over the domain. In (6) the last term, representing the active power exerted by motors on cytoskeleton filaments, is always negative. Indeed, differentiating the steady state equation for motors distribution $(w - V) = \partial_y c/c$ and multiplying it by c, we have $\int_{-\mathcal{L}/2}^{\mathcal{L}/2} c \partial_y w dy = \int_{-\mathcal{L}/2}^{\mathcal{L}/2} c \partial_y \left(\partial_y c/c\right) dy$. The desired result follows from the integration by parts of this relation $\int_{-\mathcal{L}/2}^{\mathcal{L}/2} c \partial_y w dy = -\int_{-\mathcal{L}/2}^{\mathcal{L}/2} (\partial_y c)^2/c dy < 0$. Therefore, the positivity of FV indicates that the energy dissipation (friction, viscosity) dominates the anti-dissipative power supply by the molecular motors, see [26, 44] for further details.

We remark that similar bi-directionality was also observed for other active systems [50–52]. The striking new feature of the present model is the existence of two other thresholds $\mathcal{P}_m(\mathcal{L})$ and $\mathcal{P}_s(\mathcal{L})$. For $\mathcal{P}_m < \mathcal{P}$, μ_0 becomes positive again so that the V-F curves start to display stalled states and are hysteretic under both velocity and force control. Note that for $\mathcal{P}_m < \mathcal{P} < \mathcal{P}_s$ the stall states are unstable but for $\mathcal{P} > \mathcal{P}_s$ they

stabilize. Interestingly, this type of V-F relations have been also obtained in the context of Taylor-Couettte flows of active polar fluids where the free boundaries were absent, the role of V was played by the angular velocity of the flow and the applied torque served as the analog of our F [53].

The importance of the revealed complexity of the V-F relations is demonstrated below through the solution of the two prototypical problems: active oscillations and active collision.

Active oscillations

Consider first an active segment connected to a fixed support by a spring of stiffness k_p such that

$$F(t) = -k_p x_f(t).$$

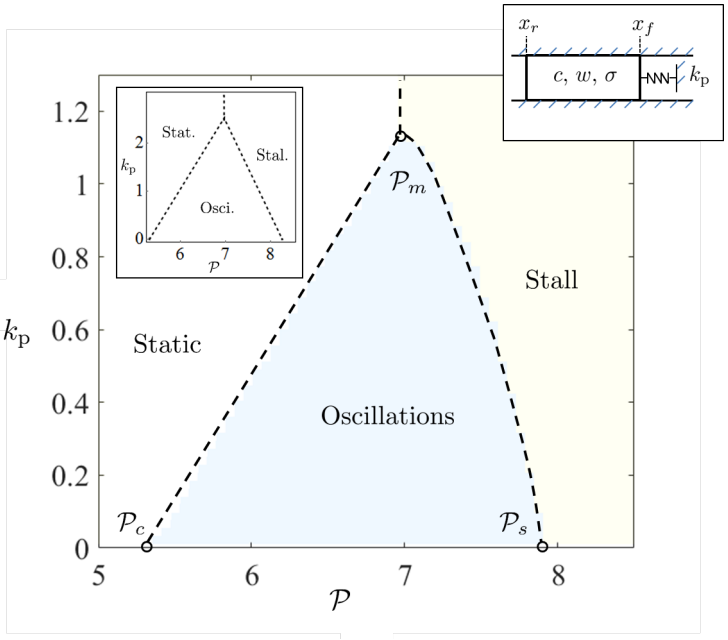

Figure 3. Numerically constructed phase diagram for the active layer tethered to a spring. Parameter $\mathcal{L} = 2$. Inset shows the phase diagram obtained with the active particle model (8) with parameters $\alpha = 12$, $k_S = 0.65$ and $k_C = 0.15$.

When $\mathcal{P} \leq \mathcal{P}_c$ such segment remains static at its equilibrium position $x_f = 0$. If, however, $\mathcal{P}_c \leq \mathcal{P} \leq \mathcal{P}_m$ and the stiffness of the spring is below a critical value $k_p^c(\mathcal{L}, \mathcal{P})$, the active segment starts to oscillate spontaneously, see Fig. 3. Behind this instability is a classical supercritical Hopf bifurcation [54]. The oscillations involve repolarization: a periodic force-induced relocation of the molecular motors from the rear to the front and back, see Fig. 4. The typical timescale of such oscillations is $\bar{t} \sim 10^3$ s (see [40]) which is realistic in view of the experimental data reported in [35].

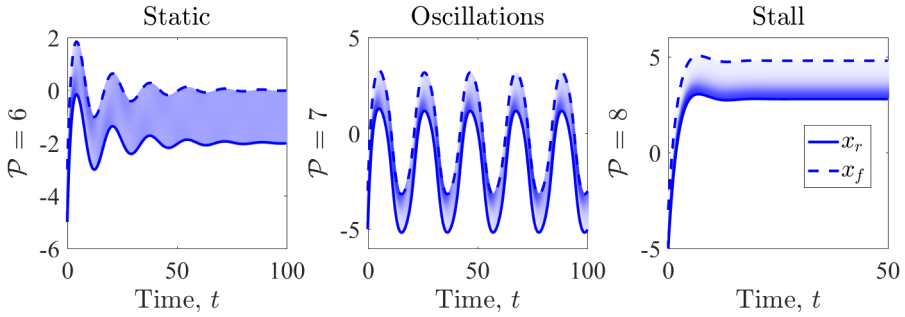

Figure 4. Three typical regimes of motion for the tethered active gel crawler, interpreted in Fig. 3 as Static, Oscillatory and Stall phases. The intensity of the coloring between the front lines is proportional to the concentration of molecular motors. Parameters: $\mathcal{L} = 2$ and $k_p = 0.6$.

The phase diagram, shown in Fig. 4 , reveals that the transition from static to oscillatory state is controlled not only by the contractility level, as it has been known experimentally [35], but also by environmental stiffness. In sufficiently stiff environments the increase of contractility can at most put the system in a stall state. In soft environments, oscillations become possible at elevated contractility with a subsequent discontinuous transition from oscillatory to stall state at even larger levels of contractility (between $\mathcal{P}_m$ and $\mathcal{P}_s$). We note that all three dynamic phases shown in Fig. 4 are accessible in soft environments by tuning contractility only, which suggests that cells in these conditions can potentially actively vary their dynamic state.

Active collision

As a second illustration, consider two identical but differently polarized active segments moving towards each other. We use the subscripts $\mp$ to differentiate the segment coming from the left (minus sign) at $t = 0$ from the segment coming from the right (plus sign), see Fig. 5. Following [10, 13], we assume that the colliding cells interact through the force F representing a repulsion potential which penalizes the overlap of the two cells:

$$F_{\pm}(\mathcal{D}) = \pm F_c \exp(-\mathcal{D}/\mathcal{D}_c). \tag{7}$$

The force F_+ is applied at the x_{r_+} boundary and F_- is symmetrically applied at the x_{f_-} boundary. The magnitude of the force depends on the degree of separation: $\mathcal{D}(t) = |x_{r_+}(t) - x_{f_-}(t)|$, see Fig. 5. In (7) we introduced a characteristic size of a cell-cell contact $\mathcal{D}_c \ll \mathcal{L}$ and defined F_c as the scale of the repulsive force.

Note that we did not impose an infinite penalization (F_c is finite) to allow the segments to pass each other. We imply that the the adhesive clusters between the two cells are only transient and that the effective spring, which engages upon the contact (i.e. when $\mathcal{D} \ll \mathcal{D}_c$), is always under compression and cannot bear any significant tensile load [38]. As cells pass each other, this spring is stretched until it disengages making the interaction force negligible at $\mathcal{D} \gg \mathcal{D}_c$. While the account of an attractive part of the interaction potential would increase the possibility of forming cell doublets and,

for many cells, would be necessary to capture the formation of a stable tissue, we leave these issues for a separate study.

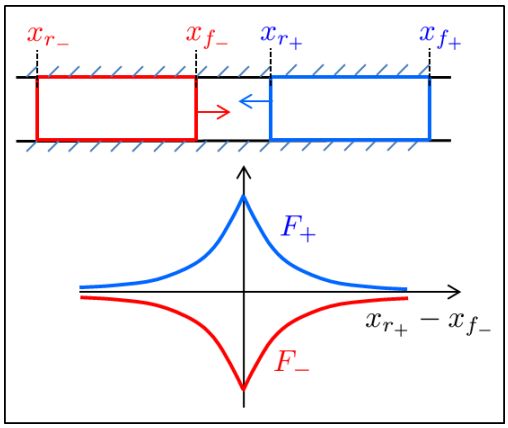

Figure 5. Scheme of the two colliding segments initially advancing towards each other and the structure of the interaction forces experienced by each of the segment.

In our numerical experiments we explored the whole range of contractility levels above the motility initiation threshold $\mathcal{P} > \mathcal{P}_c$. Similar to what was observed in experiment [36, 37], our simple mechanical model also predicts four possible outcomes of a collision test: *reversal*, pairing, which can be motile (*train*) or static (*stall*), and *bypass*. Our quantitative results are summarized in Fig. 6 showing the regimes diagram on the $(\mathcal{P}, F_c)$ plane. The typical trajectories of the colliding active agents for each of the four regimes and the corresponding configurations of molecular motors are illustrated in Fig. 7. Similar behavior was also obtained using a much more detailed biochemical model in [16].

We emphasize that in the *reversal* regimes, our active segments repolarize during collision as a result of being exposed to large contact forces. The result of such "quasi-elastic" collision is that the colliding agents change the sign of their polarities but not the magnitude of their velocities.

In the *bypass* regimes, the agents go past each other as our model allows for mutual overlap when the repulsion contact force is not sufficient to impede the propulsive machinery. While such non-one-dimensional outcomes would have to be confirmed in detailed 3D simulations, we anticipate that our prototypical model captures them adequately when the cell-cell friction is negligible compared to the cell-substrate friction.

Finally, in the pairing regimes the two initially mobile agents first get immobilized and push against each other as both of them reach transiently stall conditions. Such regimes can be stable (forming a robust *stall* phase) only for $\mathcal{P} > \mathcal{P}_s$ when there exists a steady stall state. For $\mathcal{P} < \mathcal{P}_s$, in the *train* regimes, one of the two active agents eventually sweeps along the other one by forcefully repolarizing its internal configuration and afterwards they continue traveling together as a cell doublet. One can show that in such regimes, stall configurations also exist but are unstable and are destroyed by infinitesimal perturbations.

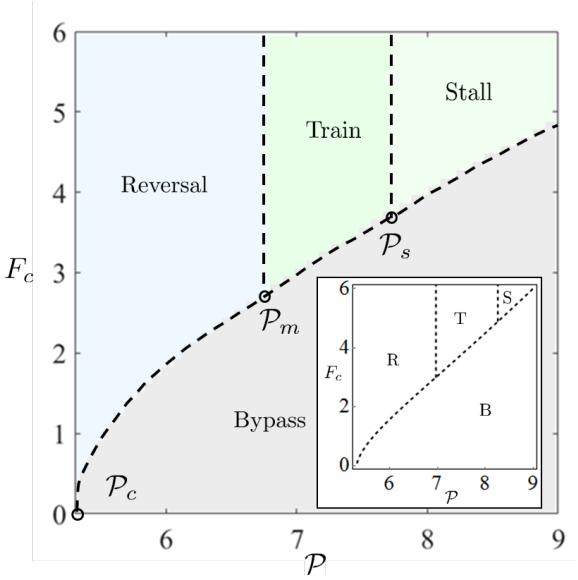

Figure 6. Phase diagram showing the four outcomes of the collision test: Reversal, Train and Pairing of cells which splits into a motile phase (Train) and a static one (Stall). Parameters are $\mathcal{L} = 2$ and $\mathcal{D}_c = 0.1$. Inset shows the phase diagram obtained within the active particle model (8) with parameters $\alpha = 12$, $k_S = 0.65$ and $k_C = 0.15$.

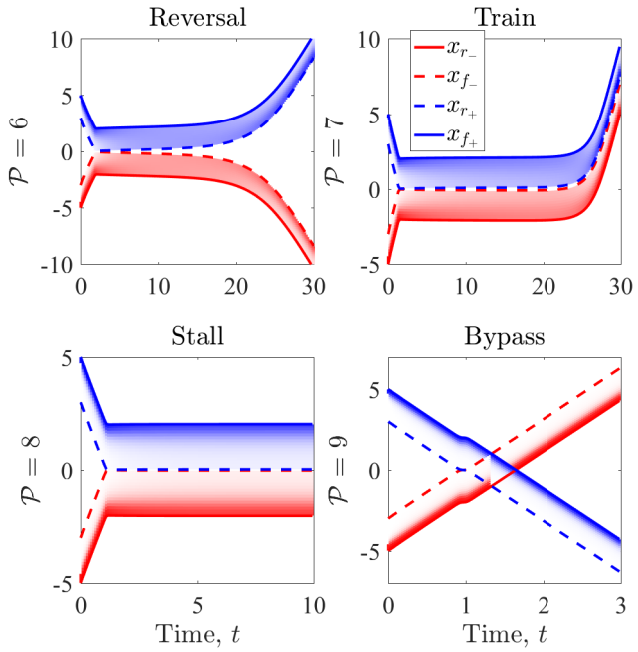

Figure 7. Typical responses and corresponding internal configurations of two colliding cells. The intensity of the coloring between the front lines is proportional to the concentration of molecular motors. Parameters: $\mathcal{L} = 2$, $\mathcal{D}_c = 0.1$ and $F_c = 4.5$.

Active particle model

To highlight the idea that the applied force affects not only the spatial location but also the polarity of a moving cell, we now construct a reduced, coarse grained model by

interpreting our active segment as an active particle. In addition to its spatial location $S(t)$ such particle should also have an internal degree of freedom $C(t)$ representing polarity. A simple reduced model can be formulated in terms of two ordinary differential equations:

$$\dot{S} = \mathcal{P}C + k_S F, \;\; \dot{C} = -\partial_C W, \tag{8}$$

where $C(t) = (\phi * c(\mathcal{L}/2, t) + \phi * c(-\mathcal{L}/2, t))/2$ is an arbitrary polarity measure and $W(C) = -k_C F C + \alpha C^4/4 - (\mathcal{P} - \mathcal{P}_c)C^2/2$ is a Landau type potential. The first equation in (8) can be derived by summing the values of velocity (5) computed at the two boundaries $\pm\mathcal{L}/2$ and using relations (1). The relation between $c(y, t)$ and $C(t)$ then follows from the averaging over the boundaries. This equation shows the competition between the external force and the active force $\mathcal{P}C$ who compete in determining the direction of the motion. The second equation in (8) is obtained phenomenologically as a way to describe spontaneous polarization at zero applied force when $\mathcal{P} = \mathcal{P}_c$ and to capture the simplest linear biasing of the polarity by the applied force.

It is remarkable that by adjusting the parameters k_S, k_C and α of this almost naive model, one can not only quantitatively mimic the hysteretic V-F relations presented in Fig. 1 but also reproduce *all* non-stationary regimes shown in Fig. 3 and Fig. 6 (see insets). The ability of the active particle model to capture the mechanical response of the active segment model points to the idea that the coupling between the polarity variable and the applied force should be an essential element of any model seeking to describe mechanical interaction of active particles with external objects.

Conclusion

We showed that a contraction-driven active gel segment exhibits fundamental bi-stability with two dynamic regimes representing opposite polarities. The associated (V-F) relations are generically doubly hysteretic, allowing for both force and velocity induced repolarization of an active object. Dynamic bi-stability was shown to play a crucial role in self-induced oscillations of a tethered active objects and to be essential for capturing the experimentally observed outcomes of the cell collision tests. Our study suggests that even the reduced model of an active particle with self-adjusting polarity is capable of describing complex mechanical cell-cell interactions. Due to its ultimate simplicity, it should prove useful for the development of the kinetic theory of tissues driven by internal cellular motion.

A major prediction of our model is that cell contractility can serve as an purely mechanical *regulator* of CIL without the need to involve complex biochemical mechano-transduction pathways. This rather unexpected result would have to be of course checked experimentally through drug treatments [55] and optogenetics [56].

Acknowledgments

P.R. acknowledges support from a CNRS-Momentum grant. T.P. was supported by the EPSRC Engineering Nonlinearity project No. EP/K003836/1. L.T. is grateful to the French government which supported his work under Grant No. ANR-10-IDEX-0001-02 PSL.

[1] Alberts B, Johnson A, Lewis J, Raff M, Roberts K and Walter P 2002 *Molecular biology of the cell* 4th ed (Garland Science Taylor & Francis Group) ISBN 0815332181
[2] Rappel W J and Edelstein-Keshet L 2017 *Current opinion in systems biology* **3** 43–53
[3] Ladoux B, Mège R M and Trepat X 2016 *Trends in cell biology* **26** 420–433
[4] Friedl P and Gilmour D 2009 *Nat. Rev. Mol. Cell Biol.* **10** 445–457
[5] Gov N 2011 *Nature Mater.* **10** 412–414
[6] Trepat X, Wasserman M, Angelini T, Millet E, Weitz D, Butler J and Fredberg J 2009 *Nature Phys.* **5** 426–430
[7] Kabla A 2012 *J. R. Soc. Interface* **9** 3268–3278
[8] Tambe D, Corey Hardin C, Angelini T, Rajendran K, Park C, Serra-Picamal X, Zhou E, Zaman M, Butler J, Weitz D, Fredberg J and Trepat X 2011 *Nature Mater.* **10** 469–475
[9] Garcia S, Hannezo E, Elgeti J, Joanny J F, Silberzan P and Gov N S 2015 *Proceedings of the National Academy of Sciences* **112** 15314–15319
[10] Löber J, Ziebert F and Aranson I S 2015 *Scientific reports* **5**
[11] Zimmermann J, Camley B A, Rappel W J and Levine H 2016 *Proceedings of the National Academy of Sciences* **113** 2660–2665
[12] Smeets B, Alert R, Pešek J, Pagonabarraga I, Ramon H and Vincent R 2016 *Proceedings of the National Academy of Sciences* **113** 14621–14626
[13] Marth W and Voigt A 2016 *Interface focus* **6** 20160037
[14] Edelstein-Keshet L, Holmes W R, Zajac M and Dutot M 2013 *Philosophical Transactions of the Royal Society of London B: Biological Sciences* **368** 20130003
[15] Merchant B, Edelstein-Keshet L and Feng J 2017 *bioRxiv* 181743
[16] Kulawiak D A, Camley B A and Rappel W J 2016 *PLoS computational biology* **12** e1005239
[17] Jülicher F, Kruse K, Prost J and Joanny J F 2007 *Physics Reports* **449** 3–28
[18] Rubinstein B, Fournier M F, Jacobson K, Verkhovsky A B and Mogilner A 2009 *Biophysical journal* **97** 1853–1863
[19] Shao D, Rappel W J and Levine H 2010 *Physical review letters* **105** 108104
[20] Ziebert F, Swaminathan S and Aranson I S 2011 *Journal of The Royal Society Interface* rsif20110433
[21] Giomi L and DeSimone A 2014 *Physical review letters* **112** 147802
[22] Tjhung E, Tiribocchi A, Marenduzzo D and Cates M 2015 *Nature communications* **6**
[23] Bois J S, Jülicher F and Grill S W 2011 *Phys. Rev. Lett.* **106**(2) 028103
[24] Recho P, Putelat T and Truskinovsky L 2013 *Phys. Rev. Lett.* **111**(10) 108102
[25] Callan-Jones A and Voituriez R 2013 *New J. Phys.* **15** 025022
[26] Recho P, Joanny J F and Truskinovsky L 2014 *Phys. Rev. Lett.* **112** 218101
[27] Maiuri P, Terriac E, Paul-Gilloteaux P, Vignaud T, McNally K, Onuffer J, Thorn K, Nguyen P A, Georgoulia N, Soong D *et al.* 2012 *Current Biology* **22** R673–R675
[28] Hawkins R J, Piel M, Faure-Andre G, Lennon-Dumenil A, Joanny J, Prost J and Voituriez R 2009 *Physical review letters* **102** 058103
[29] Doyle A D, Wang F W, Matsumoto K and Yamada K M 2009 *The Journal of cell biology* **184** 481–490
[30] Doyle A D, Petrie R J, Kutys M L and Yamada K M 2013 *Current opinion in cell biology* **25** 642–649
[31] Kruse K and Jülicher F 2005 *Current opinion in cell biology* **17** 20–26

[32] Vilfan A and Frey E 2005 *Journal of physics: Condensed matter* **17** S3901
[33] Guérin T, Prost J, Martin P and Joanny J F 2010 *Current opinion in cell biology* **22** 14–20
[34] Kruse K and Riveline D 2011 Spontaneous mechanical oscillations: implications for developing organisms *Current topics in developmental biology* vol 95 (Elsevier) pp 67–91
[35] Godeau A 2016 *Cyclic contractions contribute to 3D cell motility* Ph.D. thesis Strasbourg
[36] Desai R A, Gopal S B, Chen S and Chen C S 2013 *Journal of The Royal Society Interface* **10** 20130717
[37] Scarpa E, Roycroft A, Theveneau E, Terriac E, Piel M and Mayor R 2013 *Biology open* **2** 901–906
[38] Stramer B and Mayor R 2017 *Nature Reviews Molecular Cell Biology* **18**
[39] Davis J R, Luchici A, Mosis F, Thackery J, Salazar J A, Mao Y, Dunn G A, Betz T, Miodownik M and Stramer B M 2015 *Cell* **161** 361–373
[40] Putelat T, Recho P and Truskinovsky L 2018 *Physical Review E* **97** 012410
[41] Barnhart E L, Allen G M, Jülicher F and Theriot J A 2010 *Biophysical journal* **98** 933–942
[42] Recho P, Putelat T and Truskinovsky L 2015 *J. Mech. Phys. Solids* **84** 469–505
[43] Du X, Doubrovinski K and Osterfield M 2012 *Biophysical Journal* **102** 1738–1745
[44] Recho P and Truskinovsky L 2013 *Phys. Rev. E* **87**(2) 022720
[45] Barnhart E L, Lee K C, Keren K, Mogilner A and Theriot J A 2011 *PLoS biology* **9** e1001059
[46] Carlsson A 2011 *New journal of physics* **13** 073009
[47] Kruse K and Jülicher F 2000 *Physical review letters* **85** 1778
[48] Haines B M, Aranson I S, Berlyand L and Karpeev D A 2008 *Physical biology* **5** 046003
[49] López H M, Gachelin J, Douarche C, Auradou H and Clément E 2015 *Physical review letters* **115** 028301
[50] Jülicher F and Prost J 1995 *Physical review letters* **75** 2618
[51] Malgaretti P, Pagonabarraga I and Joanny J F 2017 *Physical review letters* **119** 168101
[52] Riveline D, Ott A, Jülicher F, Winkelmann D A, Cardoso O, Lacapère J J, Magnúsdóttir S, Viovy J L, Gorre-Talini L and Prost J 1998 *European biophysics journal* **27** 403–408
[53] Fürthauer S, Neef M, Grill S W, Kruse K and Jülicher F 2012 *New Journal of Physics* **14** 023001
[54] Guckenheimer J and Holmes P 2013 *Nonlinear oscillations, dynamical systems, and bifurcations of vector fields* vol 42 (Springer Science & Business Media)
[55] Mitrossilis D, Fouchard J, Guiroy A, Desprat N, Rodriguez N, Fabry B and Asnacios A 2009 *Proceedings of the National Academy of Sciences* **106** 18243–18248
[56] Valon L, Marín-Llauradó A, Wyatt T, Charras G and Trepat X 2017 *Nature communications* **8** 14396